PLOS PATHOGENS

RESEARCH ARTICLE

Structure-selected RBM immunogens prime polyclonal memory responses that neutralize SARS-CoV-2 variants of concern

Gonzalo Almanza[1☯], Alex E. Clark[2☯], Valentina Kouznetsova[3☯], Eduardo Olmedillas[4], Andrea Castro[5], Igor F. Tsigelny[3], Yan Wu[6], George F. Gao[7], Sandra L. Leibel[8], William Bray[9], Erica Ollmann Saphire[4], Aaron F. Carlin[2]*, Maurizio Zanetti[1]*

1 The Laboratory of Immunology, Department of Medicine and Moores Cancer Center, University of California San Diego, La Jolla, California, United States of America, **2** Division of Infectious Diseases and Global Public Health, Department of Medicine, University of California San Diego, La Jolla, California, United States of America, **3** San Diego Supercomputer Center, University of California at San Diego, La Jolla, California, United States of America, **4** Center for Infectious Disease and Vaccine Research, La Jolla Institute for Immunology, La Jolla, California, United States of America, **5** Biomedical Informatics Program, University of California San Diego, La Jolla, California, United States of America, **6** Laboratory of Pathogenic Microbiology and Immunology, Institute of Microbiology, Chinese Academy of Sciences, and School of Basic Medical Sciences, Capital Medical University, Beijing, China, **7** Laboratory of Pathogenic Microbiology and Immunology, Institute of Microbiology, Chinese Academy of Sciences, Beijing, China, **8** Department of Pediatrics, University of California San Diego School of Medicine, La Jolla, California, United States of America, **9** Division of Genetics, Department of Pediatrics, Center for Drug Discovery Innovation, Program in Immunology, Institute for Genomic Medicine, La Jolla, California, United States of America

☯ These authors contributed equally to this work.
* acarlin@health.ucsd.edu (AFC); mzanetti@health.ucsd.edu (MZ)

Abstract

Successful control of the COVID-19 pandemic depends on vaccines that prevent transmission. The full-length Spike protein is highly immunogenic but the majority of antibodies do not target the virus: ACE2 interface. In an effort to affect the quality of the antibody response focusing it to the receptor-binding motif (RBM) we generated a series of conformationally-constrained immunogens by inserting solvent-exposed RBM amino acid residues into hypervariable loops of an immunoglobulin molecule. Priming C57BL/6 mice with plasmid (p) DNA encoding these constructs yielded a rapid memory response to booster immunization with recombinant Spike protein. Immune sera antibodies bound strongly to the purified receptor-binding domain (RBD) and Spike proteins. pDNA primed for a consistent response with antibodies efficient at neutralizing authentic WA1 virus and three variants of concern (VOC), B.1.351, B.1.617.2, and BA.1. We demonstrate that immunogens built on structure selection can be used to influence the quality of the antibody response by focusing it to a conserved site of vulnerability shared between wildtype virus and VOCs, resulting in neutralizing antibodies across variants.

OPEN ACCESS

Citation: Almanza G, Clark AE, Kouznetsova V, Olmedillas E, Castro A, Tsigelny IF, et al. (2022) Structure-selected RBM immunogens prime polyclonal memory responses that neutralize SARS-CoV-2 variants of concern. PLoS Pathog 18(7): e1010686. https://doi.org/10.1371/journal.ppat.1010686

Editor: Charles R. M. Bangham, Imperial College London, UNITED KINGDOM

Received: November 9, 2021

Accepted: June 17, 2022

Published: July 21, 2022

Data Availability Statement: All relevant data are within the manuscript and its Supporting Information files.

Funding: This work was supported in part by NIH grant K08AI130381 to AFC; Burroughs Wellcome Fund Career Award for Medical Scientists to AFC; National Institutes of Health grant U19 142790-S1 to EOS; Bill and Melinda Gates Foundation INV-006133 to EOS. The funders had no role in study

design, data collection and analysis, decision to publish, or preparation of the manuscript.

Competing interests: We have read the journal's policy and the authors of this manuscript have the following competing interests: MZ is named inventor in US patent 8,372,640 that relates to the protein engineering process and method of immunization used in this work. All other authors have declared that no competing interests exist.

Author summary

Next generation SARS-CoV-2 vaccines need to address the transmission of new virus variants that continue to threaten global health and recovery. This may require new perspectives in immunogen design as well as immune response engineering. Here we applied these ideas in a two-step proof of concept study. First, we designed conformationally-constrained immunogens expressing key residues at the RBM: ACE2 interface to mimic their stereochemical orientation in the native Spike protein. Second, we initiated the process of B cell immunity (priming) using plasmid DNA injected intra-spleen to exploit the spatial organization of a secondary lymphoid organ. Mice given a single booster immunization with intact Spike protein developed a rapid memory antibody response against RBD and Spike proteins. Importantly, immune sera neutralized authentic WA1 virus and the B.1.351/Beta, B.1.617.2/Delta, and BA.1/Omicron variants of concern. Our findings demonstrate that immunogens built on structure selection and lymphoid organ targeting are a powerful way to focus the antibody response to a conserved site of vulnerability shared between wildtype virus and variants of concern.

Introduction

The current SARS-CoV-2 pandemic has been globally disruptive [1]. Nonpharmaceutical interventions (NPI) reduced viral transmission but are difficult to sustain due to deleterious social and economic consequences [https://data.undp.org]. Additionally, NPI, as implemented, have not sufficiently controlled a global pandemic that has caused more than 480 million infections and 6.1 million deaths (https://coronavirus.jhu.edu/map.html). This forced the rapid deployment of vaccines effective at mitigating the symptoms of infection but less at preventing virus transmission. Successive waves of mutations and the emergence of variants of concern (VOCs) have complicated vaccine effectiveness.

The most effective way to control infectious agents at the population level is immunization and virtually all licensed vaccines owe their protective effects to the induction of pathogen-specific antibodies [2]. Vaccine-induced antibodies protect either by preventing infection, i.e., blocking the interaction of a virus with its cell target (e.g., lung cells in the case influenza virus), or by preventing disease, i.e., blocking the virus from reaching its target organ (e.g., the central nervous system in the case of paralytic poliovirus). Cellular immunity by T cells and NK cells protect from pathology and disease by killing virus-infected cells [3] or, more generally, by limiting harmful consequences of immune activation [4]. Therefore, community spread of infection is preferably controlled by antibodies that intercept virions by preventing them from binding their receptor on target cells.

Every protein immunogen is composed of various B cell and T cell epitopes against which the immune system responds using its adaptive arm. Polyclonal antibody responses are by definition heterogeneous, driven by inter-clonal competition [5, 6], and favor the response to some epitopes at the expense of others, a phenomenon known as immunodominance [7]. As a consequence, not all epitopes in a viral pathogen induce responses beneficial to the host. For example, some antigens (e.g., nucleocapsid protein) are immunogenic and have diagnostic value [8] but the immune response against them will not prevent infection. Other epitopes suppress the immune response [9], or may induce antibodies that exacerbates pathogenesis [10]. To minimize immunodominance by irrelevant B cell epitopes and their negative impact on the immune response [6], the immune response should be controlled by narrowing the

choice of B cell epitopes involved to those with the highest probability of inducing antibodies against sites of vulnerability on the virus.

The Achilles' heel of SAR-CoV-2 for viral transmission is the interaction between the receptor binding domain (RBD) of the spike protein and the ACE2 receptor [11]. Within the RBD, the receptor binding motif (RBM) ridgeline contributes numerous key amino acid residues to the interaction with ACE2 [12, 13]. It is the target of potent neutralizing antibodies isolated from convalescent individuals via VH/VL cloning [14–21] even though >80% of the whole antibody response to the Spike protein in convalescent individuals is directed predominantly to sites outside the receptor binding domain (RBD) [22]. Furthermore, patients with mild disease and those with severe disease generate antibodies that tend to recognize different sites in the RBD [23]. Residues in the RBM involved in ACE2 contact are necessarily constrained [13] with only few common amino acid mutations in SARS-CoV-2 variants of concern in the RBM ridgeline region (for example E484K in B.1.351, T478K in B.1.617.2, and S477N, T478K, and E484A in BA.1). Although neutralizing antibodies have been mapped to the N-terminal domain [22, 24] or other sites distal from the RBM [20, 25, 26], a comprehensive study showed that all but one of the 20 most potent (IC50 < 0.1 μg/mL) neutralizing antibodies bind the RBM and block receptor attachment [27].

Here we used protein engineering to generate three plasmid (p)DNA immunogens expressing a B cell epitope of the RBM ridgeline, all comprising the ^{486}Phe-Asn-Cys-Tyr^{489} (^{486}FNCY^{489}) patch. This patch plays a key role at the RBM: ACE2 interface, is solvent-exposed, and is included in the epitope target of some of the most potent human Class 1 neutralizing antibodies [27, 28]. pDNA priming of C57BL/6 mice induced a primary and memory antibody responses against RBD. A single booster immunization expanded antibodies that were highly effective at neutralizing authentic WA1 virus, the B.1.351 and B.1.617.2 VOCs, and to a lesser degree BA.1. This approach shows that it is possible to initiate anti-SARS-CoV-2 responses recruiting B cell with receptors complementary to a narrow region of the RBM.

Results

Prime-boost immunization and serum antibody response in mice

We utilized protein engineering to express RBM amino acid sequences in the complementarity determining regions (CDRs) of the variable (V) domain of an immunoglobulin (Ig) molecule, antibody antigenization [29]. CDRs are solvent-exposed hypervariable loops supported by the conserved Ig fold [30] and independent of the physicochemical constraints that maintain the VH and VL packing. CDRs are ideal sites to express heterologous B-cell epitopes with constrained geometry imparting them with antigenicity and immunogenicity [31].

An analysis of the RBD: ACE2 interface revealed multiple contact points involving conserved residues on both sides (Fig 1A). We selected a putative B cell epitope comprising a solvent-exposed patch of four amino acid (^{486}FNCY^{489}) as a target of B cell immunity (Fig 1B) as several human Class 1 neutralizing antibodies [28] have paratopes that target this site on the RBM ridgeline (Fig 1C). We generated three immunogens (referred hereunder as Model 1–3) by inserting short RBM sequences in either CDR2 or CDR3 (Fig 1D) to evaluate local folding variability (see Material and Methods for engineering techniques). Model 2 and 3 were also designed to include the sequence QYIKANSKFIGITE, a universal T helper (Th) cell epitope from tetanus toxoid [32], in CDR3 and CDR2, respectively (S1 Fig). This epitope is not presented by the two classical class II antigens of the H2 complex I-A and I-E, and served to assess possible effects on folding of the B cell epitope and its immunogenicity.

All pDNAs are under the control of the Ig promoter so that transcription and translation of the rearranged Ig gene are restricted to B cells. The injection of pDNA into the B cell rich

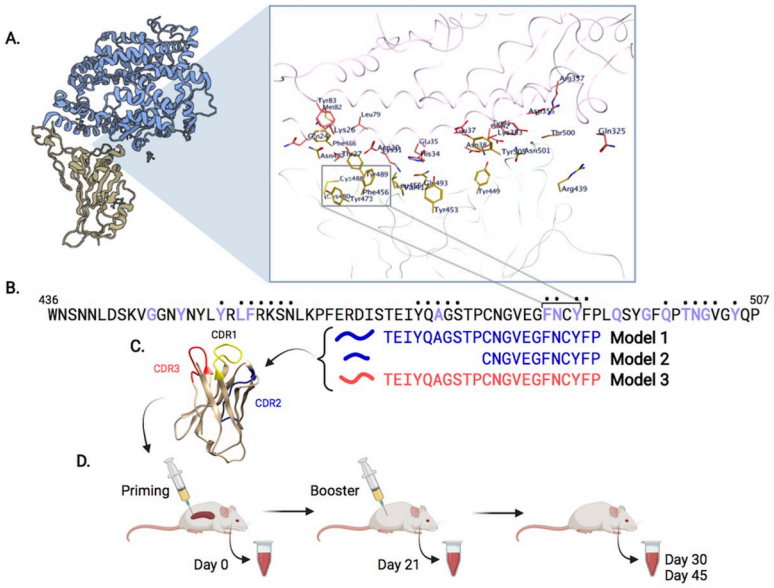

Fig 1. Overview of SARS-CoV-2 epitope selection, protein engineering, and immunization. (**A**) SARS-CoV-2 Spike protein (yellow) interacting with ACE2 (blue), PDB ID: 6M0J. A zoomed view shows SARS-CoV-2:ACE2 interacting residues. (**B**) Spike protein RBM (436–507) sequence. Purple residues indicate ACE2 binding, dots above residues indicate B38 or CC12.1 antibody binding. Immunogens models 1–3 span the putative B cell epitope FNCY (486–489). (**C**) VH62 model with CDR1 (yellow), CDR2 (blue), CDR3 (red). (**D**) Timeline of priming (day 0), and booster shot (day 21), with blood draws (days 0, 21, 30, 45). Figure adapted from images created with BioRender.com.

https://doi.org/10.1371/journal.ppat.1010686.g001

environment of the spleen leads to a process of immunity within the spatio-temporal geometry of an organized secondary lymphoid tissue, mimicking the immunodynamics of viral infection without being infectious with advantages for the formation of long-lasting immunological memory [33].

Female C57BL/6 mice (N = 4 per group) were primed by single intra-spleen injection of one of three RBM pDNAs (group = model 1–3) (Fig 1C). Mice were given a booster immunization with Spike protein (20 μg) in incomplete Freund's adjuvant (IFA) on day 21 (Fig 1D). Group 4 only received the booster immunization with Spike protein in IFA only. Sera were collected before the booster immunization and tested by ELISA on purified RBD and Spike (D614G mutation) proteins. Weak binding to RBD and Spike protein at low serum dilutions (1:50) was observed (S2 Fig), in line with the characteristics of this form of immunization [34].

The antibody response post-booster immunization was analyzed at an early (day 30) and late (day 45) time point (*i.e.*, 9 and 24 days after booster immunization), to capture the evolution of the memory response. Nine days post-booster immunization antibodies to RBD and Spike were markedly increased both in group 1 and 2, with a response also greater than that in group 3 and 4 (Fig 2). Since group 4 controls for magnitude and speed of the antibody response after booster with intact Spike protein, the data show that pDNA priming accelerated the recall antibody response by the Spike protein. Twenty-four days post-boost, the responses against the RBD and Spike proteins were considerably stronger than on day 30 and substantially similar among groups (Fig 2). We conclude that the three pDNA immunogens differed in their ability to prime a specific B cell response and generate an anamnestic response in a prime-boost regimen. A greater response against the RBM B cell epitope was associated with expression of the RBM epitope in the CDR2 loop of the VH, suggesting context-dependent immunogenicity perhaps owing to better folding and more favorable recognition by B cells relative to expression in CDR3.

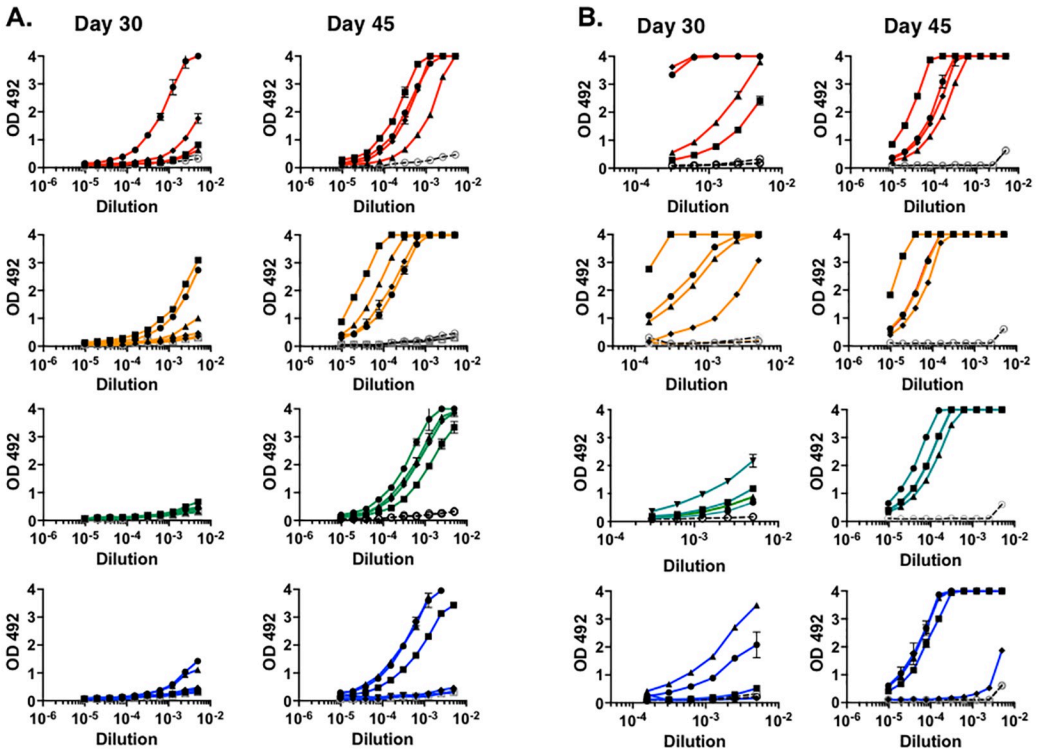

Fig 2. ELISA binding of immune sera of mice after prime-boost. Binding to RBD (**A**) and Spike protein (**B**) of sera at the timepoints indicated. Closed symbols refer to individual mice. Open symbols refer to binding of pre-immune sera. Day 30 statistical significance analysis. (RBD): group 1 vs. 4, p = 0.086; group 2 vs. 4, p = 0.054; group 3 vs. 4,—value; group 1 vs 3, p = 0.008; group 2 vs 3, p = 0.003. (Spike) group 1 vs. 4, p = 0.003; group 2 vs. 4, p = 0.009; group 3 vs. 4, p = 0.532; group 1 vs 3, p = 6.4E-06; group 2 vs 3, p = 1.69E-07. Results from one experiment representative of three independent runs each performed at different times. Sera tested in duplicate. Color scheme: red = group 1; orange = group 2; green = group 3; blue = group 4.

https://doi.org/10.1371/journal.ppat.1010686.g002

The B cell epitope selected for these studies is contained in a narrow region of the RBM. To monitor the reactivity of serum antibodies with greater precision we synthesized peptide ^{475}AGSTPCNGVEGFNCYFPLQSYGFQPT^{500}. Reactivity against the RBM peptide occurred after booster immunization with binding profiles on day 9 post-booster mimicking those on RBD and Spike proteins in groups 1 and 2, which displayed overall stronger binding relative to group 3 and 4 (S3A Fig). Intra-spleen pDNA priming induces predominantly IgM antibodies [35]. This may account for weak binding to the RBM peptide at 1:50 dilution, suggesting low antibody concentration in sera, low avidity, or both. Antibody binding increased by day 45 (S3A Fig). Thus, priming with pDNA1 and pDNA2 generated a pool of memory B cells specific for an RBM epitope comprised within residues ^{475}AGSTPCNGVEGFNCYFPLQSYGFQPT^{500} that were expanded during the anamnestic response.

Immune sera antibodies cross-compete RBD binding of neutralizing human monoclonal antibodies

The RBM amino acids grafted into CDR loops comprise contact residues shown to be targets of potently neutralizing antibodies derived from COVID-19 patients. Among those are

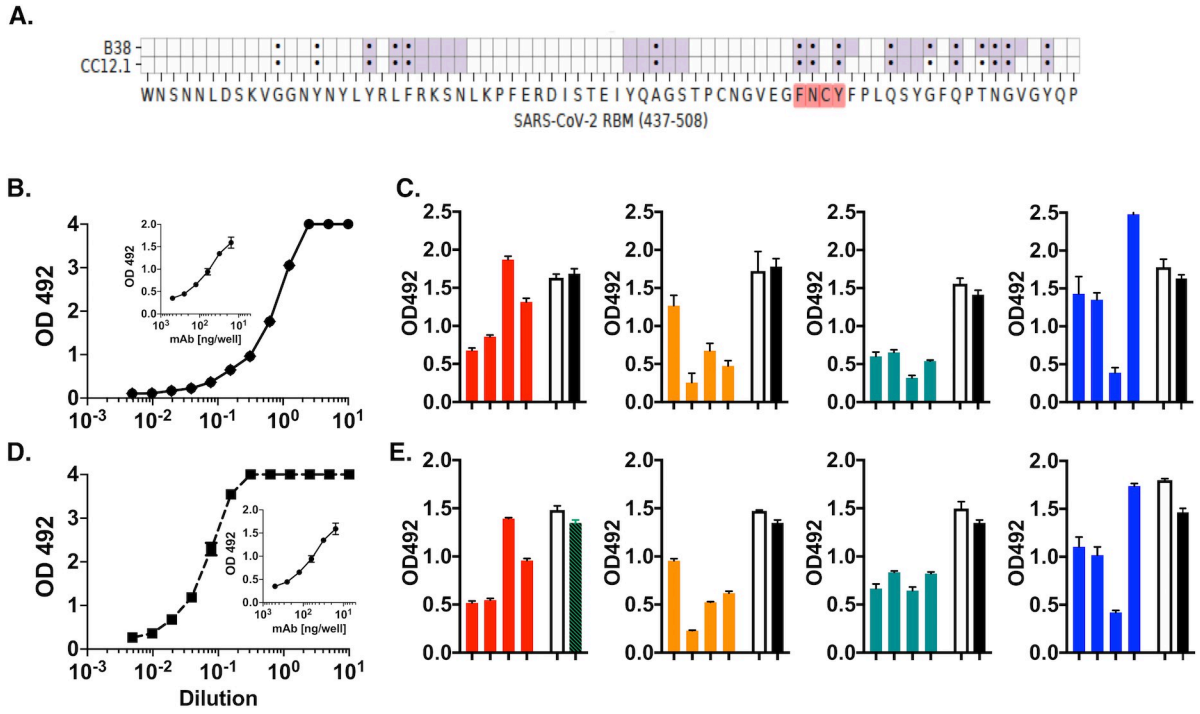

Fig 3. Polyclonal antibodies in immune sera share paratope specificity with Class 1 human neutralizing antibodies B38 and CC12.1. Immune sera were tested in a cross-competition RBD binding assay by ELISA. (**A**) Heatmap of neutralizing antibody contact residues (purple) with RBM region (positions 437–508). Black dots indicate ACE2 contact residues. (**B**) Titration of binding of HRP-B38 to RBD in ELISA. Inset: Slope of inhibition of HRP-B38 binding by unlabeled antibody B38. Effective 50% binding concentrations were (~1.5 ng/well). (**C**) Binding of HRP-B38 in the presence of 1:50 dilution of individual mouse serum (day 45). (**D**) Titration of binding of HRP-CC12.1 to RBD in ELISA. Inset: Slope of inhibition of HRP-CC12.1 binding by unlabeled antibody CC12.1. (**E**) Binding of HRP-CC12.1 in the presence of 1:50 dilution of individual mouse serum (day 45). Empty columns; pre-immune sera. Black columns indicate maximal binding of HRP-labeled antibody in ELISA buffer. Color scheme: red = group 1; orange = group 2; green = group 3; blue = group 4.

https://doi.org/10.1371/journal.ppat.1010686.g003

antibodies B38 [14] and CC12.1 [16], which map an overlapping RBM epitope including contact residues Phe—Asn and Tyr of the ^{486}FNCY^{489} patch in both cases (Fig 3A).

Our original reasoning was that the paratope of these two antibodies could be used to determine shared epitope specificity between immune serum polyclonal antibodies and human neutralizing antibodies. To this end, we designed a competitive ELISA assay where the binding of horseradish peroxidase (HRP)-labeled B38 and CC12.1 to the RBD protein was competed by individual immune sera. HRP-labeled B38 and CC12.1 bound RBD with similar characteristics (Fig 3B and 3D) so that both antibodies could be used at comparable (~1.5 ng/well) effective ~50% binding concentration. Unlabeled antibodies B38 and CC12.1 inhibited homologous RBD binding at similar concentration (50% inhibition at ~ 60 ng/well) (Fig 3B and 3D, inset).

The majority of immune sera tested individually at a 1:50 dilution inhibited >50% the binding to RBD by both HRP-B38 and HRP-CC12.1. Inhibition in group 2 was overall the strongest (range 25–85% for B38; and 30–84% for CC12.1) (Fig 3C and 3E). Surprisingly, group 3 immune sera also inhibited (range 62–80% on B38; and 38–52% on CC12.1). Group 4 had overall the weakest inhibitory activity (<30%) with the exception of one mouse. The fact that serum antibodies from immune mice cross-competed the RBD binding of the two human neutralizing antibodies indicates that a component of serum antibodies in the immune serum share the paratope with antibodies B38 and CC12.1. We estimated the upper limit serum concentration of such antibodies as high as ~12 μg/ml. Collectively, the results show that intra-

spleen priming with pDNA coding for the selected RBM epitope facilitates the booster expansion of B cell clonotypes producing RBM antibodies found in COVID-19 patients. Neither HRP-B38 nor HRP-CC12.1 bound to ^{475}AGSTPCNGVEGFNCYFPLQSYGFQPT^{500} peptide in ELISA (S3B and S3C Fig), suggesting that the synthetic peptide lacks the conformation/structure needed by the paratope of these antibodies for binding. Thus, immune sera have a wider spectrum of paratopes than those defined by the two human monoclonal antibodies.

Neutralization of authentic SARS-CoV-2 isolates WA1 and variants of concern Beta/B.1.351, Delta/B.1.617.2, and Omicron/BA.1

We tested the neutralizing activity of day 45 sera on authentic SARS-CoV-2 isolates, USA-WA1/2020 (WA1) and VOC lineages B.1.351 20H/501Y.V2/Beta (B.1.351) (Fig 4), B.1.617.2 21A/S:478K/Delta (B.1.617.2) (Fig 5), and BA.1 21K/Omicron (BA.1) (Fig 6) in a focus reduction neutralization test (FRNT) (Figs 4–7, and S4, IC_{50}s summarized in Fig 7 and Table 1). We found that sera from groups 1 and 2 gave marked neutralization of WA1 that was titratable over a 3 $\log_{10}$ dilution range with IC_{50} +/- SEM of 1:2,589 +/- 993 and 1:1,637 +/- 196, respectively. Group 3 also inhibited WA1 with an IC_{50} of 1:2,321 +/- 756. Reference group 4, which only received the booster immunization of 20μg of spike protein in IFA was neutralizing except in one case. Neutralization by control monoclonal antibodies CC12.1 and CC6.30 was strong (IC_{50} of 116 ng/ml and 8 ng/ml, respectively), consistent with published data [14, 16]. Pre-immune mouse sera did not neutralize. We then assessed neutralization of the B.1.351 VOC.

The B.1.351 variant has multiple mutations in the spike protein, including K417N, which is outside the RBD, and the E484K and N501Y mutations that are within, or immediately adjacent to, the RBM ridgeline. These mutations are also present in SARS-CoV-2 VOC P.1 and some isolates of B.1.1.7, and contribute to reduced neutralization by monoclonal antibodies, as well as convalescent and post-vaccination sera [36–38]. We noted that group 2 had consistent neutralization of B.1.351. In one instance, neutralization of both the WA1 and B.1.351 isolates was nearly superimposable (Fig 4). Group 1 sera also neutralized B.1.351 infection, but less consistently compared to wild type virus. In contrast, neutralization of the B.1.351 variant by group 3 sera was poorer. Group 4 showed strong cross-neutralization in 2 out of 4 instances. Neither monoclonal antibody CC12.1 nor CC6.30 neutralized the B.1.351 variant. Together, these results suggest that pDNA priming with the RBM epitope in CDR2 synchronizes a response to subsequent booster protein immunization that privileges recognition of both wild type SARS-CoV-2 and the B.1.351 VOC. Abrogation of neutralization of the B.1.351 VOC by monoclonal antibodies CC12.1 and CC6.30 is consistent with the key role of mutation K417N in disrupting the binding of neutralizing antibodies belonging to the Class 1 group [39].

The B.1.617.2 variant has several mutations in the spike protein, including L452R and T478K (two non ACE2 contact residues) and P681R in the S1/S2 cleavage region, but not the K417N, E484K and N501Y mutations present in the B.1.351 VOC. While again neutralization occurred in all groups we noted that group 2 had consistent neutralization of B.1.617.2, though with reduced efficacy, similarly to VOC B.1.351. In other groups, the IC_{50} for B.1.617.2 was intermediate between WA1 and B.1.351. Monoclonal antibodies CC12.1 and CC6.30 neutralized effectively as predicted by absence of the K417N mutation (Fig 5).

The Omicron variant has replaced Delta as the dominant isolate worldwide and has numerous amino acid changes in the spike protein compared to previous variants, resulting in reduced efficacy of monoclonal antibodies as well as vaccine-induced protection against infection. Groups 1 and 2 showed some neutralizing activity against BA.1 in contrast to groups 3 and 4 in which neutralization activity was completely lost (Fig 6). The comparison between

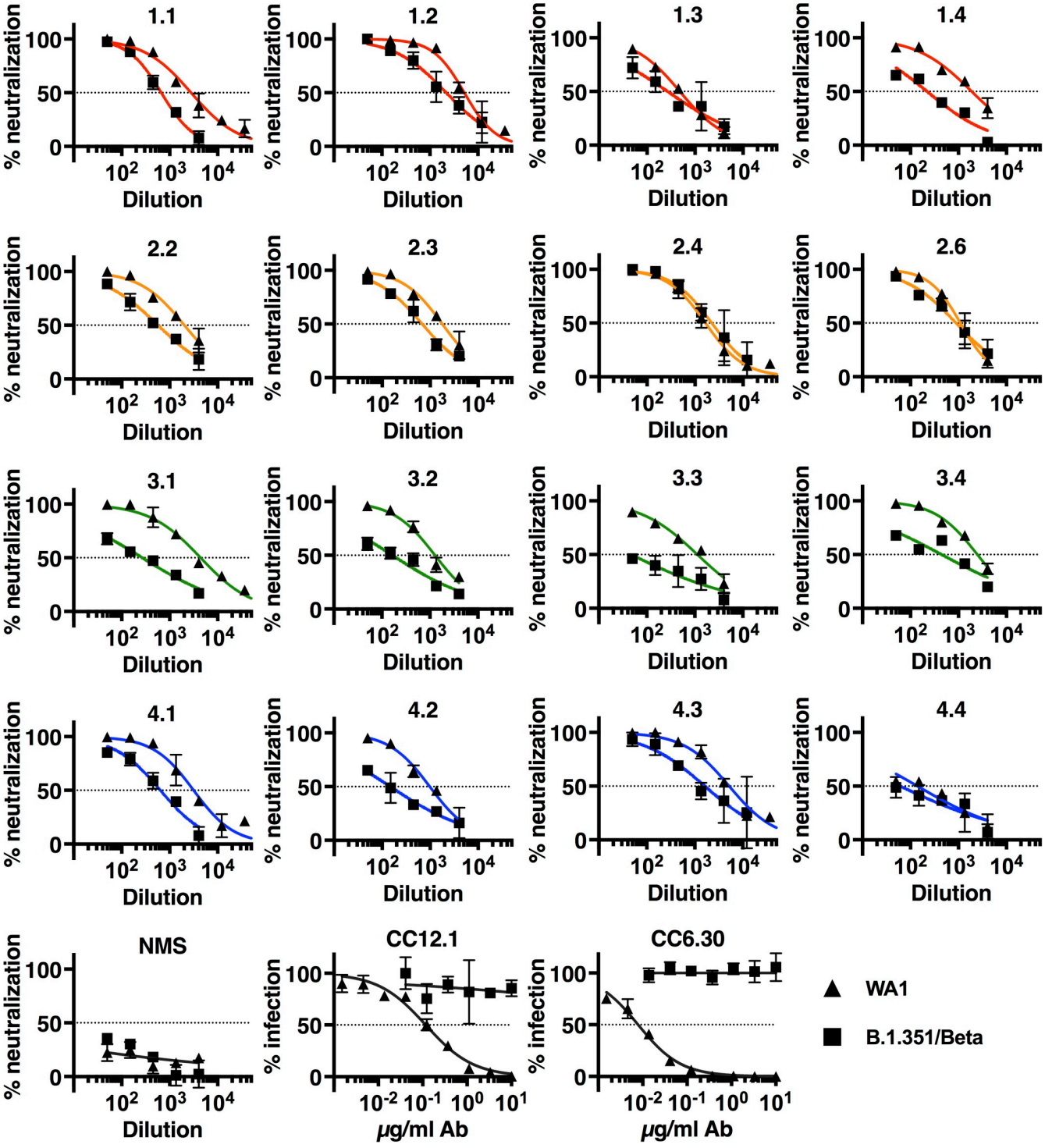

Fig 4. Neutralization of authentic SARS-CoV-2 WA1 isolate and VOCs B.1.351/Beta. Neutralization of authentic SARS-CoV-2 isolate WA1 and VOCs B.1.351 and B.1.617.2 by immune sera was measured by focus reduction neutralization test (FRNT) on TMPRSS2-Vero cells. 3-fold serial dilutions started at 1:50. Percent neutralization and percent infection are relative to media-only control. Data shown are the mean and SD of 2 biological replicates. Dotted lines mark 50% neutralization. Color scheme: red = group 1; orange = group 2; green = group 3; blue = group 4. NMS = normal mouse serum.

https://doi.org/10.1371/journal.ppat.1010686.g004

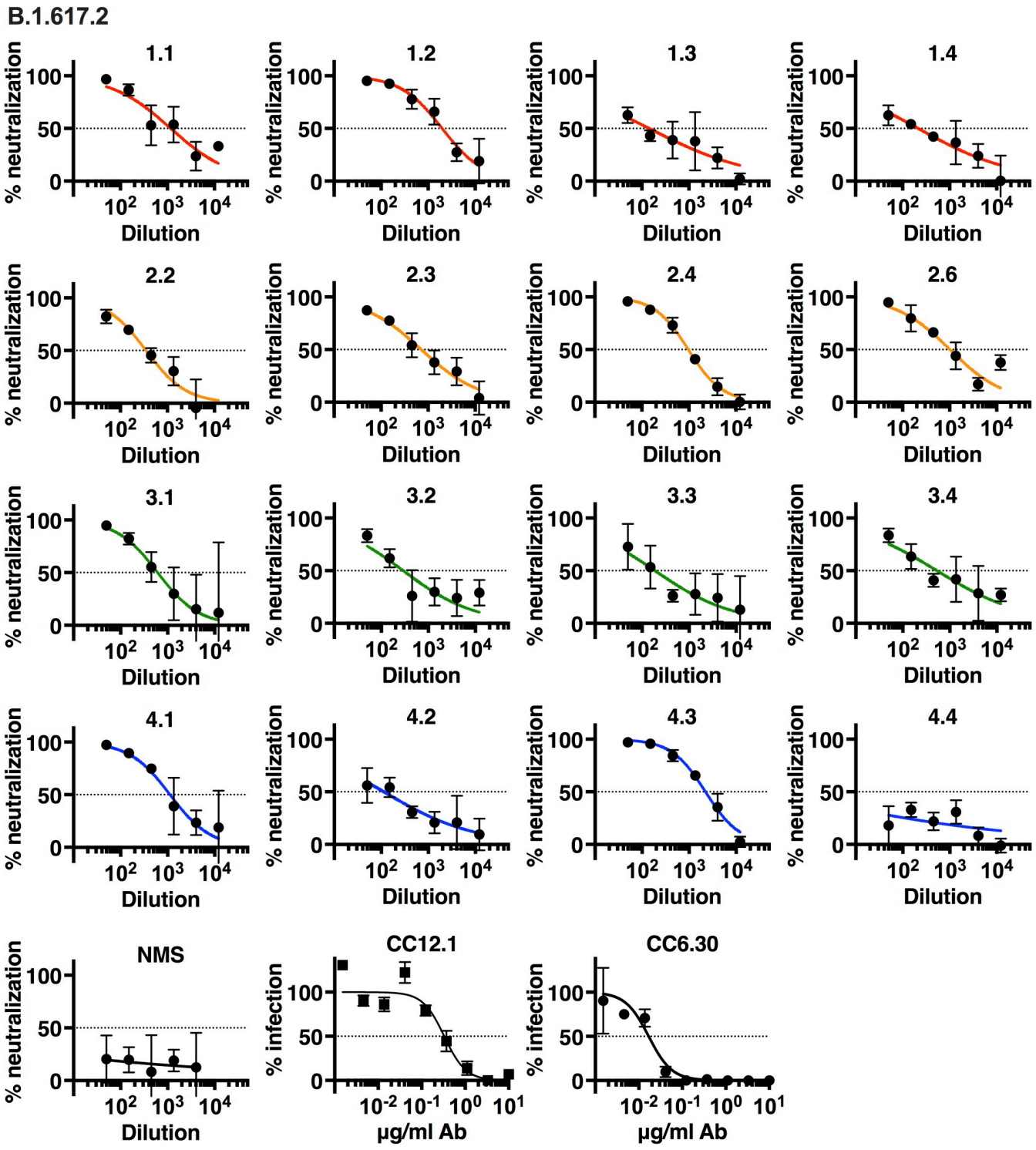

Fig 5. Neutralization of authentic SARS-CoV-2 VOC B.1.617.2/Delta isolate. Neutralization of authentic SARS-CoV-2 isolate B.1.617.2 by immune sera was measured by focus reduction neutralization test (FRNT) on TMPRSS2-Vero cells. 3-fold serial dilutions started at 1:50. Percent neutralization and percent infection are relative to media-only controls. Data shown are the mean and SD of 2–4 biological replicates. Dotted lines mark 50% neutralization. Color scheme: red = group 1; orange = group 2; green = group 3; blue = group 4. NMS = normal mouse serum.

https://doi.org/10.1371/journal.ppat.1010686.g005

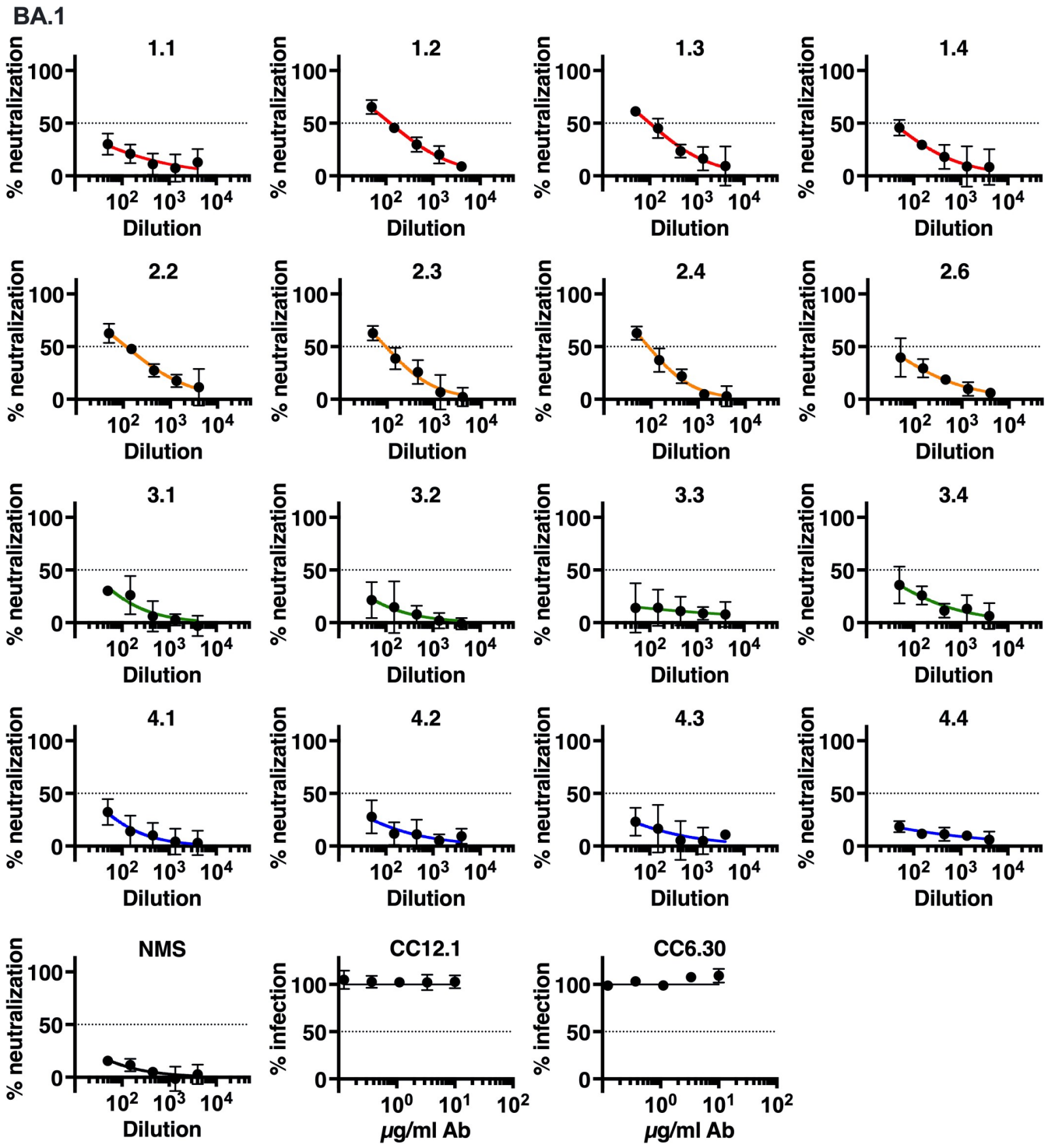

Fig 6. Neutralization of authentic SARS-CoV-2 VOC BA.1/Omicron isolate. Neutralization of authentic SARS-CoV-2 isolate BA.1 by immune sera was measured by focus reduction neutralization test (FRNT) on TMPRSS2-Vero cells. 3-fold serial dilutions started at 1:50. Percent neutralization and percent infection are relative to media-only controls. Data shown are the mean and SD of 4 biological replicates. Dotted lines mark 50% neutralization. Color scheme: red = group 1; orange = group 2; green = group 3; blue = group 4. NMS = normal mouse serum.

https://doi.org/10.1371/journal.ppat.1010686.g006

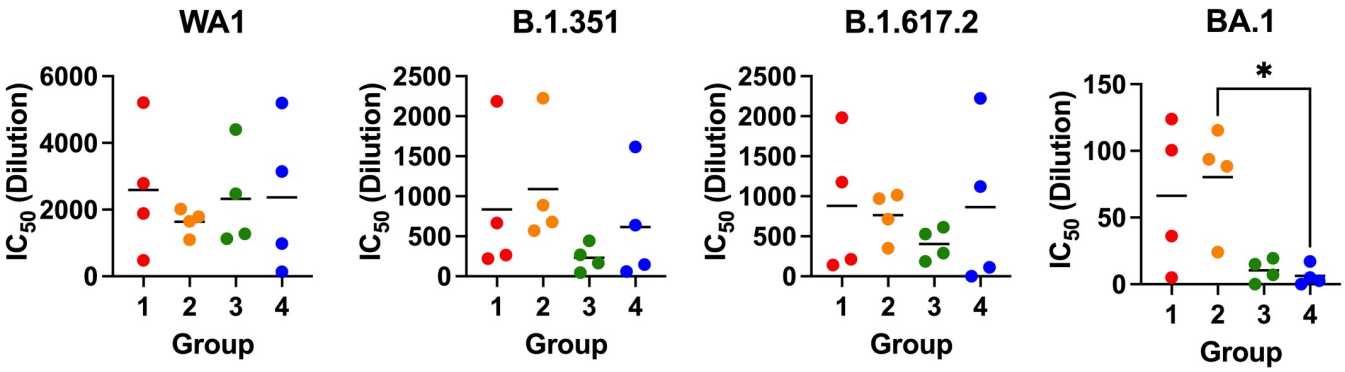

Fig 7. Comparison of IC50s from neutralization of authentic SARS-CoV-2 by immune sera from groups 1–4. IC50s from focus reduction neutralization tests (FRNTs) using the indicated variants of SARS-CoV-2 (Figs 4–6). Each point is 1 mouse. Significance determined by ordinary one-way ANOVA with comparison to reference group 4. * = $p<0.033$.

https://doi.org/10.1371/journal.ppat.1010686.g007

group 2 and group 4 achieved statistical significance (Fig 7). Neutralization of Omicron was reduced compared to other variants tested. The neutralization efficacies of groups 1 and 2 sera against B.1.351 and B.1.617.2 were reduced 1.5–3.1-fold from WA1, but were 39-fold and 20-fold reduced against BA.1 (Table 1). As predicted, antibodies CC12.1 and CC6.30 did not neutralize BA.1.

In conclusion, we demonstrate that immune mice sera neutralize not only authentic WA1 virus but also VOCs responsible for rapid spreading of infection and disease. The neutralization of BA.1 by Group 1 and in particular Group 2 was superior to immunization with spike alone and only 20 fold reduced over WA1 in Group 2.

Structure-function considerations on B cell epitope expression

We used computer modeling techniques to model the RBM B cell epitope ^{480}CNGVEGFNCYFP^{491} expressed in the CDR2 of Model 2 as mice primed with pDNA 2 provided the most consistent antibody response and neutralized authentic wild type virus, and the B.1.351 and B.1.617.2 and to a lesser extent BA.1 VOCs. Model 2 expresses RBM epitope in the CDR2 region and the sequence QYIKANSKFIGITE, a universal T helper epitope from the tetanus toxoid (TT) in CDR3. However, since TT epitope is not presented by I-A and I-E class II antigens of the H2 complex, its presence is only relevant to folding and immunogenicity of the RBM B cell epitope.

Table 1. IC50s from neutralization of authentic SARS-CoV-2 VOCs and fold-reduction in neutralization efficacy compared with WA1 variant.

	IC50 WA1	SEM WA1	IC50 B.1.351	SEM B.1.351	IC50 B.1.617.2	SEM B.1.617.2	IC50 BA.1	SEM BA.1	IC50 B.1.351 foldΔ from WA1	IC50 B.1.617.2 foldΔ from WA1	IC50 BA.1 foldΔ from WA1
Group 1	2589	993	835	461	879	437	66	28	3.1	2.9	39.0
Group 2	1637	196	1091	384	763	153	80	20	1.5	2.1	20.4
Group 3	2321	756	231	84	404	99	10	4	10.0	5.7	223.4
Group 4	2364	1136	616	357	864	518	6	4	3.8	2.7	379.5

IC50s were derived from neutralization curves in Figs 4–6. IC50s were determined by nonlinear curve fit as described in Material and Methods.

https://doi.org/10.1371/journal.ppat.1010686.t001

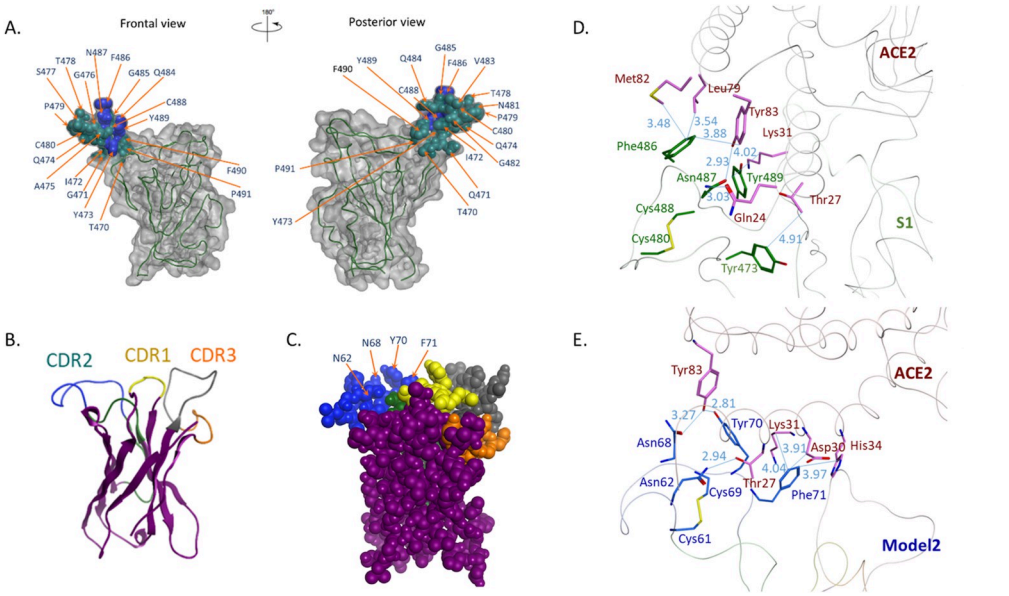

Fig 8. Conformational analysis of SARS2-CoV-2 RBM structure and predicted conformation of VH Model 2. In the Spike S1 protein (**A**) the tip of the RBM ridgeline is shown in dark green and the FNCY patch in dark blue. In Model 2 (ribbon **B**) and (space filling **C**) the modeled CDR2 loop is shown in dark green, while the grafted RBM epitope is in dark blue. Panels on the right show the interface between ACE2 and SARS-CoV-2 RBM (**D**), and ACE2 and the CDR2 loop of Model 2 (**E**). Color scheme: A: gray—RBD; green—RBM; blue–ACE2 contact residues; B and C: yellow -CDR1; green—CDR2; orange—CDR3; blue—SARS-Cov-2 RBM residues grafted in CDR2; gray—tetanus toxoid epitope; D: pink—ACE2; green—SARS-Cov-2 RBM residues; E: pink—ACE2; blue—SARS-Cov-2 RBM residues grafted in CDR2.

https://doi.org/10.1371/journal.ppat.1010686.g008

As seen in Fig 8B and 8C, the orientation of the RBM epitope, notably the ^{486}FNCY^{489} patch, is projecting outward and is solvent-exposed as in the Spike 1 protein (Fig 8A). Examining the docking interactions between the Phe-Asn-Tyr triad and ACE2 residues (Fig 8D and 8E and S1 Table) it appears that the RBM epitope expressed in the CDR2 loop establishes a greater number of shorter distance binding interactions with ACE2, suggesting an overall stereochemical similarity with the corresponding residues of the ^{486}FNCY^{489} patch in the virus RBM. Thus, a favorable surface exposure and spatial orientation of the B cell epitope centered on the ^{486}FNCY^{489} patch support the immunogenicity of Model 2 pDNA.

Discussion

We engineered three immunogens expressing a B cell epitope of the RBM ridgeline in the CDR loops of an Ig V domain scaffold as immunogens against SARS-CoV-2. The B cell epitope spans a small region (22 amino acids) of the RBM ridgeline and encompasses the solvent-exposed ^{486}FNCY^{489} patch, which contributes three contact residues to ACE2 receptor binding [12]. Numerous human Class 1 neutralizing antibodies [28], including B38 and CC12.1, have been mapped to this region [14, 16]. We used a DNA-protein (heterologous prime-boost) approach to screen pDNAs able to prime an antibody response against RBD and induce a memory response. We show that two of the three pDNAs tested, both expressing the RBM B cell epitope in CDR2, induced a strong neutralizing response not only against the WA1 isolate but also the B.1.351 and B.1.617.2, and to a lesser degree, BA.1 VOCs.

After protein booster immunization, polyclonal serum antibodies (group 1 and 2) bound the RBD and the Spike proteins and also synthetic peptide ^{475}AGSTPCNGVEGFNCYFPLQSYGFQPT^{500}. ELISA titers at the early (day 30) expansion of the memory response correlated

with a consistent virus neutralization on day 45 (group 2), suggesting a rapid anamnestic expansion of B cells specific for the minimal RBM B cell epitope ^{480}CNGVEGFNCYFP^{491}. Analysis of day 45 immune sera showed strong binding to RBD and Spike proteins, but also inhibition of binding to RBD by two potently neutralizing human antibodies (B38 and CC12.1) reported to map to an overlapping site in the RBM ridgeline (Fig 3A). This suggests that some among the polyclonal antibodies in immune sera shared epitope specificity with these two human neutralizing antibodies. However, neither antibody B38 nor CC12.1 bound peptide ^{475}AGSTPCNGVEGFNCYFPLQSYGFQPT^{500}, suggesting that polyclonal antibodies induced in mice via pDNA-protein heterologous immunization have multiple paratope specificities and unlike antibodies B38 and CC12.1 their binding to the RBM B cell epitope is independent of residue K417 [39]. An alternative explanation is that their paratopes bind from a different angle.

Polyclonal antibodies in immune sera after prime-boost immunization neutralized efficiently authentic SARS-CoV-2 WA1, B.1.351, and B.1.617.2, and with some efficacy BA.1 isolates. Although neutralization of wild type virus was expected in light of the strong ELISA antibody titers against RBD and Spike proteins, neutralization of the B.1.351, B.1.617.2, and BA.1 VOCs, particularly by group 2 sera, was not. Compellingly, this shows that few critical solvent-exposed amino acids in the RBM can expand B cells with a paratope specific for the RBM. One may argue that neutralization of the VOCs by polyclonal antibodies in immune sera is owed to recognition of a discrete epitope within the RBM that is conserved among the WA1 virus and the VOCs considered in this study: B.1.351, B.1.617.2, and BA.1. In line with this interpretation Wang et al. [40] showed that potent neutralizing antibodies in convalescent individuals that utilize the IGVH1.58 germline gene have similar potency against the B.1.351 and B.1.617.2 variants. Some of these antibodies (A23-58.1 and B1.182.1) map to a "supersite" that is overlapping with the minimal RBM B cell epitope ^{480}CNGVEGFNCYFP^{491} characterized in the present study. Additional examples of supersite antibodies have been reported such as antibody SE12 [21, 41] and antibody S2K146 [42] (Fig 9). Interestingly, antibody S2K146 acts through ACE2 molecular mimicry. Collectively, this shows that when this B cell epitope is conformationally-constrained in the CDR2 is not only immunogenic but also captures a spectrum of paratopes efficient at neutralizing across the WA1 virus, and the B.1.351, B.1.617.2,

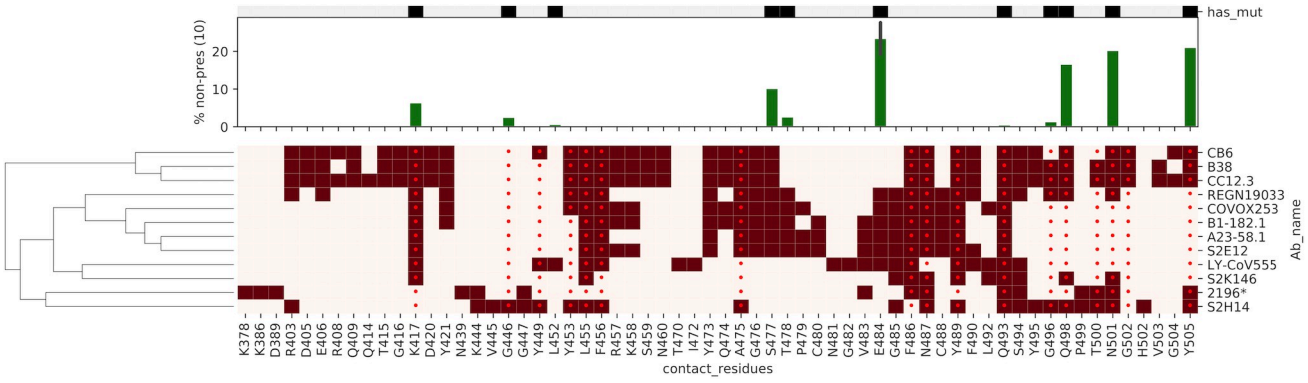

Fig 9. Overview of key amino acid residues in the RBM in or around the ^{486}Phe-Asn-Cys-Tyr^{489} "FNCY" patch. The heatmap shows neutralizing antibodies clustered by contact residues (dark red squares), and their relation to ACE2 binding residues (red dots). The middle barplot shows the percentage of all MHC-II alleles that can now not effectively present a mutated residue compared to wildtype with a threshold of a NetMHCIIpan rank of 10. The top plot indicates which residues are mutated in the parental/WA1, Beta, Delta, and Omicron Variants of Concern. For discussion on antibodies A23-58.1 [40], B1.182.1 [40], SE12 [21, 41], and S2K146 [42] see text.

https://doi.org/10.1371/journal.ppat.1010686.g009

and BA.1 variants of concern. This stresses the importance of defining immunogenic sites at the structure/function level for efficient precision immunization.

Our study has limitations. First, the sample size was deliberately low since the study was designed to identify (a) pDNA with ability to prime RBM-specific B cells that could be re-expanded during a recall response, and (b) yield consistent virus neutralization. Since the experiment was originally designed, waves of VOCs emerged, posing challenges to cross-neutralization. Our data suggest that the strategy described herein proved effective in controlling the antibody response to VOCs as moving targets. It also suggests that the polyclonal antibody response recapitulates that of few monoclonal antibodies found to recognize a conserved RBM epitope vulnerable to mutations, for example E484 and S477, which affect the binding of most antibodies induced by infection or vaccination. In spite of this limitation, we managed to identify an immunogen yielding an overall consistent response. Second, the dose of Spike protein used in the booster immunization was probably excessive as this protein is highly immunogenic. This may have masked the true potential of the memory response. Future experiments will need to assess memory responses against booster immunization with lower doses of antigen. Finally, although we identified a prime-boost combination able to influence the quality of the anti-RBD antibody response, yielding neutralizing antibodies effective at blocking the RBM -ACE2 interaction of the wildtype virus and three VOCs (B.1.351, B.1.617.2, and BA.1), the results cannot be extrapolated to predict transmission inhibition *in vivo*. This needs to be the next step to validate this approach.

Current vaccines have greatly mitigated the severity of disease caused by emerging variants, but have failed to block infection and spread (contagion). Continued responses to COVID-19 and to future pandemics rest on an effective immunological intervention to curb the spread of infection by vaccination, inducing durable transmission-blocking immunity. The initial evidence gathered in this study suggests that a pDNA-protein (prime-boost) approach was successful in focusing the antibody response to a narrow site of the RBM ridgeline that overlaps with the RBM supersite recently described [40] and proved effective against wildtype virus and three VOCs (B.1.351, B.1.617.2, and BA.1). This suggests that binding and neutralization mediated by polyclonal antibodies in immune sera is likely enriched in antibodies binding the RBM supersite. Our data also show that the E484K mutation which is present in the B.1.351 VOC and shared by another VOC (P.1/Gamma or 20J/501Y.V3) as well as several variants of interest (B.1.525, P.2, P.3, and some isolates of B.1.526) does not block the reactivity of antibodies generated in our prime-boost immunization. This contrasts studies showing that antibodies induced by natural infection or vaccines based on wildtype Spike are less effective at neutralizing the B.1.351 variant [38, 43–48], leading potentially to immune escape. It also contrasts with the fact that monoclonal antibodies, and vaccinated and convalescent sera, have much (>80%) decreased neutralization potency against Omicron (BA.1) [49, 50]. Since Omicron RBM mutations (K417N, N4400K, G446S, S477N, T478K, E484A, Q493R, G496S, Q498R, N501Y, and Y505H) spare the core ^{486}FNCY^{489} patch, it is not surprising that a single booster immunization enriched for antibodies to the B cell supersite neutralization against Omicron. Various reports show that the residual neutralization after two vaccine doses is 180 fold less potent compared to WA virus [51]. Similarly, the immune sera raised against whole spike protein was nearly 380-fold less neutralizing to BA.1 than to WA1 (Table 1). However, the prime boost strategy with groups 1 and 2 yielded 39- and 20-fold less potent responses to BA.1 than to WA1, a marked improvement.

The results presented here show that immunogens expressing a preselected site of the RBM ridgeline can focus the antibody response to the RBM. The need to do so is emphasized by the fact that > 80% of the whole antibody response in humans is directed predominantly to sites outside the RBD [22] consistent with the observation that B and T cell responses targeting the

RBD, and in particular the RBM, are a minority of the total response to the S protein [52]. However, all but one of 20 most potent neutralizing antibodies (IC50 < 0.1 μg/mL) characterized to date bind the RBM and block receptor attachment [27].

The type of immunogens tested here were designed to prime the antibody response against a selected site in the RBM ridgeline, which appears to overlap with the RBM site later found to be the target of broadly neutralizing antibodies [21, 40–42] (Fig 9). We also tested the hypothesis that protective B cell immunity initiated within the spatial structure of a secondary lymphoid organ as the site of immune induction is effective at selecting B cell clonotypes for expansion by booster immunization, suggesting a way to control the outcome of immunization. Therefore, it will be important to develop delivery strategies that mimic the approach demonstrated here. Added advantages of the immune engineering approach presented herein are the possibility to (i) co-express B cell epitopes mapping to additional sites of vulnerability of the virus, and (ii) limit the expansion of B cells clones selected on immunodominance [6] that may reactivate the production of pathogenetic autoantibodies [53–55] and cause immune suppression [9].

Achieving global control of this pandemic will require vaccines that overcome obstacles such as antigen stability, vaccine thermostability, and the logistics of cold chain requirements [56, 57]. pDNA vaccines of the type presented here offer such a possibility if they are incorporated in thermostable needle-free delivery vehicles for global and equitable vaccination [58].

Materials and methods

Experimental design

The experimental design is illustrated in Fig 1. The overall objective of the study was to identify an immunogen able to prime a polyclonal response expandable as a memory response upon boost immunization while enriching for antibodies recognizing a specific site in the RBM ridgeline.

Recombinant proteins, monoclonal antibodies and synthetic peptide

The generation of SARS-CoV-2 HexaPro Spike variant D614G and soluble RBD (sRBD) was performed as follows. SARS-CoV-2 HexaPro ectodomain containing residues 14–1208 (Genbank: MN908947) with the mutation D614G was stabilized in the prefusion conformation by the introduction of six proline substitutions (F817P, A892P, A899P, A942P, K986P, V987P), the replacement of cleavage site residues 682–685 ("RRAR" to "GSAS"), and the introduction of a C-terminal Foldon trimerization domain. For the generation of a soluble version of the SARS-CoV-2 RBD, one gene encoding amino acids 319–591 from the Wuhan variant was used. Both proteins HexaPro and sRBD were then cloned into a phCMV mammalian expression vector containing an N-terminal Gaussia luciferase signal sequence (MGVKVLFALICIAVAEA) and two C-terminal Strep-Tags for the purification of the proteins. Between the proteins and the purification tags an HRV-3C cleavage site was introduced to enzymatically remove the tags after the purification if necessary. Plasmids were transformed into Stellar competent cells and isolated using a Plasmid Plus Midi kit (Qiagen). Transient transfection and protein purification were performed as follows. Briefly, SARS-CoV-2 Spike ectodomain and the sRBD were transiently transfected in Freestyle ExpiCHO-S cells (Thermo Fisher). ExpiCHO cells were maintained and transfected according to the manufacturer using the "High Titer" protocol. Briefly, plasmid DNA and Expifectamine were mixed in Opti-PRO SFM (Gibco) according to the manufacturer's instructions and added to the cells. One day after the transfection, cells were fed with manufacturer-supplied feed and enhancer as specified in the manufacturer's according to protocol, and cultures were set to 32˚C, 5% CO_2 and 115 RPM.

One week later, supernatants were clarified by centrifugation, BioLock was added, passaging through a 0.22 μM sterile filter, and proteins were first purified on an ÄKTA go system (Cytivia) using a 5mL StrepTrap-HP column equilibrated with TBS buffer (25mM Tris pH 7.6, 200mM NaCl, 0.02% $NaN_3$3) and eluted using TBS buffer supplemented with 5mM d-Desthiobiotin (Sigma Aldrich). Proteins were then second purified by size-exclusion-chromatography (SEC) on a Superdex 6 increase 10/300 column (Cytivia) in the same TBS buffer. Human monoclonal antibodies B38, CC12.1 and CC6.30 have been described previously [14, 16]. The RBM peptide ^{475}AGSTPCNGVEGFNCYFPLQSYGFQPT^{500} was synthesized by Synthetic Biomolecules (San Diego) and purified by HPLC (>90% purity).

Protein engineering methods

Engineering methods were a modification of those described in [59]. Briefly, the three VH genes matching the descriptions of Model 1–3 as shown in Fig 1 were synthesized with unique ends for cloning into the ZUC1.1 (9.7 Kb) target vector using the cloning site as shown in S5 Fig. The ZUC1.1 plasmid lacks Amp resistance gene and SV40 sequences and is optimized for human use. The amino acid sequences of the Variable domain of Model 1–3 are shown in S1 Fig. pDNAs were prepared from transformed DH5a *Escherichia coli* according to standard procedures and were analyzed for purity using the following equation: %N = (11.1R-6.32)/(2.16-R) where R = 260nm/280nm, %N = % of nucleic aci. pDNAs were resuspended in sterile saline solution and stored at –20˚C until use.

Mice and immunizations

Twelve-week-old female C57Bl/6 (H-2^b) were bred at the University of California, San Diego animal facility where they were kept throughout the performance of the experiment. Mice were primed by single intra-spleen inoculation of 100 μg of plasmid DNA in 50 μl of sterile saline solution. Booster immunization was administered on day 21 after priming by a 2–3 subcutaneous injections on the back of purified Spike protein (20 μg per mouse) emulsified in incomplete Freunds' adjuvant (IFA). Procedures were per protocol approved by the Institutional Animal Care and Use Committee (IACUC) and in compliance with Association for Assessment Accreditation of Laboratory Animal Care (AAALAC) International guidelines.

Serologic assays

Direct ELISA. Antibodies to Spike, RBD and RBM peptide were detected by ELISA on 96-well polyvinyl microtiter plate (Dynatech, Gentilly, VA) coated with Spike (4 μg/ml) or RBD (4 μg/ml) proteins, or RBM peptide (6 μg/ml) in carbonate buffer pH 8.6, 0.1M, by incubation overnight at +4˚C. After coating, wells were blocked with 5% BSA in PBS for 1 hour at 37 C. Mouse sera were diluted in phosphate buffered saline (PBS) 0.15 M, pH 7.3, with 1% bovine serum albumin (BSA) and 0. 5% Tween-20 and then incubated overnight at +4˚C. The bound antibodies were revealed using a HRP-conjugated goat antibody to mouse Ig absorbed with human Ig (Sigma) (1:4,000 dilution). The bound peroxidase was revealed by adding o-phenylenediamine dihydrochloride and H_2O_2. Plates were read after 30 minutes in a micro-plate reader (TECAN Spark plate reader) at 492 nm. Tests were run in duplicate and repeated 2–3 time for consistency. Competition ELISA. (1) The detection of antibodies in immunized sera with shared epitope recognition with human monoclonal antibodies B38 and CC12.1 was performed as follows. Briefly, B38 (10 μg) and CC12.1 (100 μg) were coupled with HRP using the ab 102890 –HRP Conjugation kit (Lightning Link, Abcam) following the manufacturer's instructions. Sera from individual mice (1:100 dilution or otherwise specified) in PBS-BSA containing 0.5% Tween-20, were incubated overnight with a dilution of HRP-B38 or

HRP-CC12. 1 (~2.5 ng/ml) at +4˚C on 96-well plates coated with RBD protein (4 μg/ml). Binding was revealed as described above.

SARS-CoV-2 viruses

All work with SARS-CoV-2 was conducted in Biosafety Level-3 containment at the University of California San Diego following the guidelines approved by the Institutional Biosafety Committee. SARS-CoV-2 isolates WA1(USA-WA1/2020, NR-52281) and B.1.351/Beta (hCoV-19/South Africa/KRISP-K005325/2020, NR-54009) were acquired from BEI and passaged once through primary human bronchial epithelial cells (NHBECs) differentiated at air-liquid interface (ALI) to select against furin site mutations. Culture and differentiation of NHBECs at ALI are described below. Viruses were then expanded by one passage through TMPRSS2-Vero cells (Sekisui XenoTech). Isolate B.1.617.2/Delta (hCoV-19/USA/PHC658/2021, NR-55611) was expanded on TMPRSS2-Vero cells. Supernatants were clarified and stored at -80˚C and titers were determined by fluorescent focus assay on TMPRSS2-Vero cells. Isolate BA.1/Omicron strain hCoV-19/USA/CA-SEARCH-59467/2021 was isolated from a patient sample under UC San Diego IRB #160524 with sequence deposited at GISAID (EPI_ISL_8186377). Serial dilutions in DMEM + 3% FBS were made from a positive nasopharyngeal swab stored in viral transport media. Dilutions were incubated on TMPRSS2-Vero cells and monitored for CPE. When CPE was observed, the contents were transferred to fresh cells for a total of 3 passages on TMPRSS2-Vero cells. All viral stocks are verified by full genome sequencing.

Primary normal human airway epithelial cell culture and differentiation at air-liquid interface

Primary normal human bronchial epithelial cells (NHBECs) were obtained from a 65 year old Caucasian male without identifiers sourced from Lonza (NHBE CC-2540; Walkersville, MD). The NHBECs were revived from cryopreservation and expanded with PneumaCult Ex-Plus media (StemCell #05040, Tukwila, WA). 50,000 cells were seeded on transwells (Corning #29442–082, VWR) pre-coated with 50ug/mL Collagen type I from Rat tail (BD Biosciences #354236) at 7.5ug/cm2 in PneumaCult Ex-Plus media. Media was changed on days 1 and 3. On Day 4–7, the apical and basolateral chambers were fed PneumaCult ALI media (StemCell #05021) supplemented with 10μM ROCK inhibitor (Tocris Y-27632). Upon reaching confluency, the apical media was removed (airlift) and the basal media replaced with PneumaCult ALI media without Y-27632. Subsequent media changes were every 2–3 days thereafter. On Day 14 post-airlift, the apical surfaces were washed with DPBS once per week. Cells were grown in 37˚C, 5% CO_2 incubator until four weeks airlifted.

Infection of NHBECs at air liquid interface

After two 30 min incubations with PBS at 37˚C, 5% CO_2, virus diluted in PBS was added to apical chambers in 100uL. Virus was removed after 24h and apical washes (150uL PBS with 10 min incubation at 37˚C, 5% CO_2,) were taken daily and stored at -80. Titers were determined by fluorescent focus assay on TMPRSS2-Vero cells.

Authentic virus neutralization assay

Neutralizing antibodies in immune sera were screened through the focus reduction neutralization test (FRNT). Briefly, ~100 focus forming units (ffu) of SARS-CoV-2 were incubated with or without serially diluted sera or antibodies for 1 hour in DMEM with 1% FBS at 37˚C before

adding to 100% confluent TMPRSS2-Vero cell monolayers in 96 well plates. After 1 hour incubation at 37˚C with rocking, inocula were removed and monolayers overlaid with 100μl of DMEM + 2% FBS containing 1% methylcellulose. After 1 day incubation (37˚C) cells were fixed with 4% formaldehyde and stained with antibody against nucleocapsid protein (GeneTex, gtx135357). Whole-well images of stained foci + phase contrast were acquired at 4x magnification on an Incucyte S3, and foci were counted using the software tools onboard the Incucyte. Neutralization was calculated as the percentage of reduced foci compared to the mean of the foci in virus media-only control wells on each plate. All data is the average +/- SD of 2–4 biological replicates. In one case in which foci had begun to merge, % neutralization was computed using total area of nucleocapsid staining instead of automated count. This method was found to produce comparable results to a blinded manual count. Best fit curves generated in PRISM 9 determined the serum dilution which achieved 50% focus reduction (IC_{50}).

Computational modeling

Computational models utilized the coordinates of rearranged murine VH62 [60]. Model predictions have been made using SWISS-MODEL, an automated protein structure homology-modelling server and the coordinates of the crystal structure of an antibody: antigen complex (SMTL ID: 5mhe.1) where the antibody is specific for L-Thyroxine, which is also the epitope specificity of monoclonal antibody 62 from which VH62 was originally cloned [60]. Structure predictions of the SARS-CoV-2 RBM B-cell epitope CNGVEGFNCYFP inserted in CDR2 were made using Loop Modeler application of Molecular Operating Environment (MOE) program (Chemical Computing Group, Montreal, Canada). Modeler application employs two methods for generating the possible backbone conformations of a loop: a *de novo* method and a knowledge-based approach using crystal structures from the PDB (Chemical Computing Group. MOE 2019.01. Manuals and Tutorials: Loop/Linker Modeler and Browser). All generated loop conformations are scored using an initial scoring based on backbone atoms only. In our model we used the PDB search methodology implemented in the Loop Modeler application of MOE, version 2019.0102.

Three parameters are used for input: (1) the distance between Cα atoms in the anchor residues in the input structure; (2) the desired loop sequence, which determines a loop length and geometry restriction; and (3) whether the search is for an outgap or a loop (An outgap is defined as being either the N–or C–terminal ends of a chain. A loop is defined as a series of sequential residues in the interior of a chain) [61]. A set of variants were subsequently generated. Selected conformation of Model 2 antibody was saved. Model 2 CDR3 was engineered by insertion of the universal T helper (Th) cell epitope from tetanus toxoid QYIKANSKFIGITE and was modified using Loop Modeler of MOE. The CDR1 was not modified after SWISS--MODEL. Then the entire antibody model was docked to the ACE2 protein, using Dock module of MOE software and the interface analyzed to elucidate the interacting residues of both proteins.

Quantification of data and statistical analysis

ELISA data were plotted using GraphPad Prism version 9.1. Statistical comparison among groups, top values of each group (n = 8) was performed using student's t-test scipy version 1.3.1. Data plotting and statistical analyses of FRNT authentic virus neutralization assays were done in GraphPad Prism 9.0. Best fit curves were determined by normalized variable slope non-linear curve fit. Ordinary one-way ANOVA with comparison of each group to reference group 4 was performed to compare group IC_{50}s.

Supporting information

S1 Fig. Amino acid sequence of VH domain of Model 1–3. In red are indicated the inserts of RBM residues. In blue is indicated the tetanus toxoid sequence inserted in CDRs.
(TIF)

S2 Fig. Binding to RBM and Spike protein of sera from day 21 pDNA primed mice. Sera were tested at 1:50 dilution. In duplicate on 96 well microtiter plates coated with RBD (4 μg/ml) or Spike (4 μg/ml). Groups are color-coded as follows: Red (Group 1); Orange (Group 2); Green (Group 3); Grey (pre-immune sera). Statistical comparison among groups: (RBD) 1 vs 2 = ns; 1 vs 3 = ns; 2 vs 3 = ns; (Spike) 1 vs 2 = ns; 1 vs 3 p = 0.009; 2 vs 3 = ns. A second run showed no significant difference among groups. (ns = not significant).
(TIF)

S3 Fig. Binding to RBM peptide by mouse immune sera and human neutralizing monoclonal antibodies. A. Binding of serial serum dilutions of immune sera of the day 30 and 45 bleeds on 96-well microtiter plates coated with RBM synthetic peptide ^{475}AGSTPCNGVEGFNCYFPLQSYGFQPT^{500}. B. Binding of HRP-labeled B38 (top) and CC12.1 (bottom) to RBM peptide or RBD protein as indicated. C. Picture of ELISA assay corresponding to the slopes shown in panel B.
(TIF)

S4 Fig. Examples of images of focus reduction neutralization test (FRNT). FRNT was performed as described in Materials and Methods. After staining cell monolayers with antibody against nucleocapsid, whole wells were imaged and foci counted using Incucyte S3 with onboard software tools. Phase contrast images of whole wells (not shown) were acquired to confirm integrity of cell monolayers. Example shows assay of monoclonal antibody CC12.1 and normal mouse serum (NMS) control.
(TIF)

S5 Fig. Diagram of Zuc1.1 plasmid. It shows plasmid size, regulatory elements present, and cloning sites in the VH region. Not to scale.
(TIF)

S1 Table. Docking results from solution of SASR-CoV-2 RBM and Engineered loop of Model 2 complexed with ACE2.
(TIF)

Acknowledgments

The authors thank Dr. Dennis Burton (The Scripps Research Institute, La Jolla, CA) for the generous gift of purified human monoclonal antibodies CC12.1 and CC6.30. We thank the UC San Diego Center for Advanced Laboratory Medicine Clinical Microbiology and Virology Lab and UC San Diego EXCITE for providing clinical samples for viral isolation and SARS-CoV-2 genome sequencing. The following reagent was deposited by the Centers for Disease Control and Prevention and obtained through BEI Resources, NIAID, NIH: SARS-Related Coronavirus 2, Isolate USA-WA1/2020, NR-52281. The following reagent was obtained through BEI Resources, NIAID, NIH: SARS-Related Coronavirus 2, Isolate hCoV-19/South Africa/KRISP-K005325/2020, NR-54009, contributed by Alex Sigal and Tulio de Oliveira. The following reagent was obtained through BEI Resources, NIAID, NIH: SARS-Related Coronavirus 2, Isolate hCoV-19/USA/PHC658/2021 (Lineage B.1.617.2; Delta Variant), NR-55611, contributed by Dr. Richard Webby and Dr. Anami Patel.

Author Contributions

Conceptualization: Maurizio Zanetti.

Formal analysis: Gonzalo Almanza, Alex E. Clark, Valentina Kouznetsova.

Funding acquisition: Erica Ollmann Saphire, Aaron F. Carlin, Maurizio Zanetti.

Investigation: Gonzalo Almanza, Alex E. Clark, Valentina Kouznetsova, Eduardo Olmedillas, Yan Wu, William Bray.

Methodology: Valentina Kouznetsova.

Project administration: Maurizio Zanetti.

Resources: Eduardo Olmedillas, Sandra L. Leibel, William Bray.

Software: Valentina Kouznetsova.

Supervision: Igor F. Tsigelny, George F. Gao, Sandra L. Leibel, Erica Ollmann Saphire.

Visualization: Alex E. Clark, Valentina Kouznetsova, Andrea Castro.

Writing – original draft: Alex E. Clark, Valentina Kouznetsova, Andrea Castro, Igor F. Tsigelny, Aaron F. Carlin, Maurizio Zanetti.

Writing – review & editing: Alex E. Clark, Valentina Kouznetsova, Erica Ollmann Saphire, Aaron F. Carlin, Maurizio Zanetti.

References

1. Nicola M, Alsafi Z, Sohrabi C, Kerwan A, Al-Jabir A, Iosifidis C, et al. The socio-economic implications of the coronavirus pandemic (COVID-19): A review. Int J Surg. 2020; 78:185–93. Epub 2020/04/20. https://doi.org/10.1016/j.ijsu.2020.04.018 PMID: 32305533; PubMed Central PMCID: PMC7162753.
2. Plotkin SA. Correlates of protection induced by vaccination. Clin Vaccine Immunol. 2010; 17(7):1055–65. Epub 2010/05/14. https://doi.org/10.1128/CVI.00131-10 PMID: 20463105; PubMed Central PMCID: PMC2897268.
3. Sridhar S, Begom S, Bermingham A, Hoschler K, Adamson W, Carman W, et al. Cellular immune correlates of protection against symptomatic pandemic influenza. Nat Med. 2013; 19(10):1305–12. Epub 2013/09/24. https://doi.org/10.1038/nm.3350 PMID: 24056771.
4. de Jong MD, Simmons CP, Thanh TT, Hien VM, Smith GJ, Chau TN, et al. Fatal outcome of human influenza A (H5N1) is associated with high viral load and hypercytokinemia. Nat Med. 2006; 12 (10):1203–7. Epub 2006/09/12. https://doi.org/10.1038/nm1477 PMID: 16964257; PubMed Central PMCID: PMC4333202.
5. Kuraoka M, Schmidt AG, Nojima T, Feng F, Watanabe A, Kitamura D, et al. Complex Antigens Drive Permissive Clonal Selection in Germinal Centers. Immunity. 2016; 44(3):542–52. Epub 2016/03/08. https://doi.org/10.1016/j.immuni.2016.02.010 PMID: 26948373; PubMed Central PMCID: PMC4794380.
6. Altman MO, Angeletti D, Yewdell JW. Antibody Immunodominance: The Key to Understanding Influenza Virus Antigenic Drift. Viral Immunol. 2018; 31(2):142–9. Epub 2018/01/23. https://doi.org/10.1089/vim.2017.0129 PMID: 29356618; PubMed Central PMCID: PMC5863095.
7. Cirelli KM, Carnathan DG, Nogal B, Martin JT, Rodriguez OL, Upadhyay AA, et al. Slow Delivery Immunization Enhances HIV Neutralizing Antibody and Germinal Center Responses via Modulation of Immunodominance. Cell. 2019; 177(5):1153–71 e28. Epub 2019/05/14. https://doi.org/10.1016/j.cell.2019.04.012 PMID: 31080066; PubMed Central PMCID: PMC6619430.
8. Burbelo PD, Riedo FX, Morishima C, Rawlings S, Smith D, Das S, et al. Sensitivity in Detection of Antibodies to Nucleocapsid and Spike Proteins of Severe Acute Respiratory Syndrome Coronavirus 2 in Patients With Coronavirus Disease 2019. J Infect Dis. 2020; 222(2):206–13. Epub 2020/05/20. https://doi.org/10.1093/infdis/jiaa273 PMID: 32427334; PubMed Central PMCID: PMC7313936.
9. Xu H, Zhang L, Heyman B. IgG-mediated immune suppression in mice is epitope specific except during high epitope density conditions. Sci Rep. 2018; 8(1):15292. Epub 2018/10/18. https://doi.org/10.1038/s41598-018-33087-6 PMID: 30327481; PubMed Central PMCID: PMC6191431.

10. Arvin AM, Fink K, Schmid MA, Cathcart A, Spreafico R, Havenar-Daughton C, et al. A perspective on potential antibody-dependent enhancement of SARS-CoV-2. Nature. 2020; 584(7821):353–63. Epub 2020/07/14. https://doi.org/10.1038/s41586-020-2538-8 PMID: 32659783.

11. Altmann DM, Boyton RJ. COVID-19 vaccination: The road ahead. Science. 2022; 375(6585):1127–32. Epub 2022/03/11. https://doi.org/10.1126/science.abn1755 PMID: 35271316.

12. Lan J, Ge J, Yu J, Shan S, Zhou H, Fan S, et al. Structure of the SARS-CoV-2 spike receptor-binding domain bound to the ACE2 receptor. Nature. 2020; 581(7807):215–20. Epub 2020/04/01. https://doi.org/10.1038/s41586-020-2180-5 PMID: 32225176.

13. Starr TN, Greaney AJ, Hilton SK, Ellis D, Crawford KHD, Dingens AS, et al. Deep Mutational Scanning of SARS-CoV-2 Receptor Binding Domain Reveals Constraints on Folding and ACE2 Binding. Cell. 2020; 182(5):1295–310 e20. Epub 2020/08/26. https://doi.org/10.1016/j.cell.2020.08.012 PMID: 32841599; PubMed Central PMCID: PMC7418704.

14. Wu Y, Wang F, Shen C, Peng W, Li D, Zhao C, et al. A noncompeting pair of human neutralizing antibodies block COVID-19 virus binding to its receptor ACE2. Science. 2020; 368(6496):1274–8. Epub 2020/05/15. https://doi.org/10.1126/science.abc2241 PMID: 32404477; PubMed Central PMCID: PMC7223722.

15. Shi R, Shan C, Duan X, Chen Z, Liu P, Song J, et al. A human neutralizing antibody targets the receptor-binding site of SARS-CoV-2. Nature. 2020; 584(7819):120–4. Epub 2020/05/27. https://doi.org/10.1038/s41586-020-2381-y PMID: 32454512.

16. Rogers TF, Zhao F, Huang D, Beutler N, Burns A, He WT, et al. Isolation of potent SARS-CoV-2 neutralizing antibodies and protection from disease in a small animal model. Science. 2020; 369(6506):956–63. Epub 2020/06/17. https://doi.org/10.1126/science.abc7520 PMID: 32540903; PubMed Central PMCID: PMC7299280.

17. Barnes CO, West AP Jr., Huey-Tubman KE, Hoffmann MAG, Sharaf NG, Hoffman PR, et al. Structures of Human Antibodies Bound to SARS-CoV-2 Spike Reveal Common Epitopes and Recurrent Features of Antibodies. Cell. 2020; 182(4):828–42 e16. Epub 2020/07/10. https://doi.org/10.1016/j.cell.2020.06.025 PMID: 32645326; PubMed Central PMCID: PMC7311918.

18. Zost SJ, Gilchuk P, Case JB, Binshtein E, Chen RE, Nkolola JP, et al. Potently neutralizing and protective human antibodies against SARS-CoV-2. Nature. 2020; 584(7821):443–9. Epub 2020/07/16. https://doi.org/10.1038/s41586-020-2548-6 PMID: 32668443.

19. Liu L, Wang P, Nair MS, Yu J, Rapp M, Wang Q, et al. Potent neutralizing antibodies against multiple epitopes on SARS-CoV-2 spike. Nature. 2020; 584(7821):450–6. Epub 2020/07/23. https://doi.org/10.1038/s41586-020-2571-7 PMID: 32698192.

20. Pinto D, Park YJ, Beltramello M, Walls AC, Tortorici MA, Bianchi S, et al. Cross-neutralization of SARS-CoV-2 by a human monoclonal SARS-CoV antibody. Nature. 2020; 583(7815):290–5. Epub 2020/05/19. https://doi.org/10.1038/s41586-020-2349-y PMID: 32422645.

21. Tortorici MA, Beltramello M, Lempp FA, Pinto D, Dang HV, Rosen LE, et al. Ultrapotent human antibodies protect against SARS-CoV-2 challenge via multiple mechanisms. Science. 2020; 370(6519):950–7. Epub 2020/09/26. https://doi.org/10.1126/science.abe3354 PMID: 32972994; PubMed Central PMCID: PMC7857395.

22. Voss WN, Hou YJ, Johnson NV, Delidakis G, Kim JE, Javanmardi K, et al. Prevalent, protective, and convergent IgG recognition of SARS-CoV-2 non-RBD spike epitopes. Science. 2021; 372(6546):1108–12. Epub 2021/05/06. https://doi.org/10.1126/science.abg5268 PMID: 33947773.

23. Ravichandran S, Lee Y, Grubbs G, Coyle EM, Klenow L, Akasaka O, et al. Longitudinal antibody repertoire in "mild" versus "severe" COVID-19 patients reveals immune markers associated with disease severity and resolution. Sci Adv. 2021; 7(10). Epub 2021/03/07. https://doi.org/10.1126/sciadv.abf2467 PMID: 33674317; PubMed Central PMCID: PMC7935365.

24. Chi X, Yan R, Zhang J, Zhang G, Zhang Y, Hao M, et al. A neutralizing human antibody binds to the N-terminal domain of the Spike protein of SARS-CoV-2. Science. 2020; 369(6504):650–5. Epub 2020/06/24. https://doi.org/10.1126/science.abc6952 PMID: 32571838; PubMed Central PMCID: PMC7319273.

25. Yuan M, Wu NC, Zhu X, Lee CD, So RTY, Lv H, et al. A highly conserved cryptic epitope in the receptor binding domains of SARS-CoV-2 and SARS-CoV. Science. 2020; 368(6491):630–3. Epub 2020/04/05. https://doi.org/10.1126/science.abb7269 PMID: 32245784; PubMed Central PMCID: PMC7164391.

26. Lv Z, Deng YQ, Ye Q, Cao L, Sun CY, Fan C, et al. Structural basis for neutralization of SARS-CoV-2 and SARS-CoV by a potent therapeutic antibody. Science. 2020; 369(6510):1505–9. Epub 2020/07/25. https://doi.org/10.1126/science.abc5881 PMID: 32703908; PubMed Central PMCID: PMC7402622.

27. Dejnirattisai W, Zhou D, Ginn HM, Duyvesteyn HME, Supasa P, Case JB, et al. The antigenic anatomy of SARS-CoV-2 receptor binding domain. Cell. 2021; 184(8):2183–200 e22. Epub 2021/03/24. https://doi.org/10.1016/j.cell.2021.02.032 PMID: 33756110; PubMed Central PMCID: PMC7891125.

28. Barnes CO, Jette CA, Abernathy ME, Dam KA, Esswein SR, Gristick HB, et al. SARS-CoV-2 neutralizing antibody structures inform therapeutic strategies. Nature. 2020; 588(7839):682–7. Epub 2020/10/13. https://doi.org/10.1038/s41586-020-2852-1 PMID: 33045718; PubMed Central PMCID: PMC8092461.

29. Zanetti M. Antigenized antibodies. Nature. 1992; 355:466–77.

30. Wu TT, Kabat EA. J Exp Med. 1970; 132:211. https://doi.org/10.1084/jem.132.2.211

31. Zanetti M, Billetta R. Antigenized antibodied from concept to applications. In "The Antibodies" Zanetti M. and Capra J.D. Eds. Amsterdam: Hardwood Academic Publishers; 1996; 2: 75–121.

32. Panina BP, Tan A, Termijtelen A, Demotz S, Corradin G, Lanzavecchia A. Universally immunogenic T cell epitopes: promiscuous binding to human MHC class II and promiscuous recognition by T cells. Eur J Immunol. 1989; 19(12):2237–42. https://doi.org/10.1002/eji.1830191209 PMID: 2481588

33. Zanetti M, Castiglioni P, Rizzi M, Wheeler M, Gerloni M. B lymphocytes as antigen-presenting cell-based genetic vaccines. Immunol Rev. 2004; 199:264–78. Epub 2004/07/06. https://doi.org/10.1111/j.0105-2896.2004.00152.x PMID: 15233740.

34. Gerloni M, Baliou WR, Billetta R, Zanetti M. Immunity to Plasmodium falciparum malaria sporozoites by somatic transgene immunization. Nat Biotechnol. 1997; 15(9):876–81. https://doi.org/10.1038/nbt0997-876 PMID: 9306403.

35. Gerloni M, Lo D, Zanetti M. DNA immunization in relB-deficient mice discloses a role for dendritic cells in IgM—>IgG1 switch in vivo. Eur J Immunol. 1998; 28(2):516–24. https://doi.org/10.1002/(SICI)1521-4141(199802)28:02<516::AID-IMMU516>3.0.CO;2-M PMID: 9521061.

36. Weisblum Y, Schmidt F, Zhang F, DaSilva J, Poston D, Lorenzi JC, et al. Escape from neutralizing antibodies by SARS-CoV-2 spike protein variants. Elife. 2020; 9. Epub 2020/10/29. https://doi.org/10.7554/eLife.61312 PMID: 33112236; PubMed Central PMCID: PMC7723407.

37. Garcia-Beltran WF, Lam EC, St Denis K, Nitido AD, Garcia ZH, Hauser BM, et al. Multiple SARS-CoV-2 variants escape neutralization by vaccine-induced humoral immunity. Cell. 2021; 184(9):2372–83 e9. Epub 2021/03/21. https://doi.org/10.1016/j.cell.2021.03.013 PMID: 33743213; PubMed Central PMCID: PMC7953441.

38. Wang P, Nair MS, Liu L, Iketani S, Luo Y, Guo Y, et al. Antibody resistance of SARS-CoV-2 variants B.1.351 and B.1.1.7. Nature. 2021; 593(7857):130–5. Epub 2021/03/09. https://doi.org/10.1038/s41586-021-03398-2 PMID: 33684923.

39. Yuan M, Huang D, Lee CD, Wu NC, Jackson AM, Zhu X, et al. Structural and functional ramifications of antigenic drift in recent SARS-CoV-2 variants. Science. 2021; 373(6556):818–23. Epub 2021/05/22. https://doi.org/10.1126/science.abh1139 PMID: 34016740; PubMed Central PMCID: PMC8284396.

40. Wang L, Zhou T, Zhang Y, Yang ES, Schramm CA, Shi W, et al. Ultrapotent antibodies against diverse and highly transmissible SARS-CoV-2 variants. Science. 2021; 373(6556). Epub 2021/07/03. https://doi.org/10.1126/science.abh1766 PMID: 34210892.

41. Starr TN, Czudnochowski N, Liu Z, Zatta F, Park YJ, Addetia A, et al. SARS-CoV-2 RBD antibodies that maximize breadth and resistance to escape. Nature. 2021; 597(7874):97–102. Epub 2021/07/15. https://doi.org/10.1038/s41586-021-03807-6 PMID: 34261126.

42. Park YJ, De Marco A, Starr TN, Liu Z, Pinto D, Walls AC, et al. Antibody-mediated broad sarbecovirus neutralization through ACE2 molecular mimicry. Science. 2022; 375(6579):449–54. Epub 2022/01/07. https://doi.org/10.1126/science.abm8143 PMID: 34990214.

43. Shen X, Tang H, Pajon R, Smith G, Glenn GM, Shi W, et al. Neutralization of SARS-CoV-2 Variants B.1.429 and B.1.351. New England Journal of Medicine. 2021; 384(24):2352–4. Epub 2021/04/08. https://doi.org/10.1056/NEJMc2103740 PMID: 33826819; PubMed Central PMCID: PMC8063884.

44. Jangra S, Ye C, Rathnasinghe R, Stadlbauer D, Personalized Virology Initiative study g, Krammer F, et al. SARS-CoV-2 spike E484K mutation reduces antibody neutralisation. Lancet Microbe. 2021. Epub 2021/04/14. https://doi.org/10.1016/S2666-5247(21)00068-9 PMID: 33846703; PubMed Central PMCID: PMC8026167.

45. Liu Y, Liu J, Xia H, Zhang X, Fontes-Garfias CR, Swanson KA, et al. Neutralizing Activity of BNT162b2-Elicited Serum. New England Journal of Medicine. 2021; 384(15):1466–8. Epub 2021/03/09. https://doi.org/10.1056/NEJMc2102017 PMID: 33684280; PubMed Central PMCID: PMC7944950.

46. Wu K, Werner AP, Koch M, Choi A, Narayanan E, Stewart-Jones GBE, et al. Serum Neutralizing Activity Elicited by mRNA-1273 Vaccine. New England Journal of Medicine. 2021; 384(15):1468–70. Epub 2021/03/18. https://doi.org/10.1056/NEJMc2102179 PMID: 33730471; PubMed Central PMCID: PMC8008744.

47. Cele S, Gazy I, Jackson L, Hwa SH, Tegally H, Lustig G, et al. Escape of SARS-CoV-2 501Y.V2 from neutralization by convalescent plasma. Nature. 2021; 593(7857):142–6. Epub 2021/03/30. https://doi.org/10.1038/s41586-021-03471-w PMID: 33780970.

48. Collier DA, De Marco A, Ferreira I, Meng B, Datir RP, Walls AC, et al. Sensitivity of SARS-CoV-2 B.1.1.7 to mRNA vaccine-elicited antibodies. Nature. 2021; 593(7857):136–41. Epub 2021/03/12. https://doi.org/10.1038/s41586-021-03412-7 PMID: 33706364.

49. Nabel KG, Clark SA, Shankar S, Pan J, Clark LE, Yang P, et al. Structural basis for continued antibody evasion by the SARS-CoV-2 receptor binding domain. Science. 2022; 375(6578):eabl6251. Epub 2021/12/03. https://doi.org/10.1126/science.abl6251 PMID: 34855508.

50. Mannar D, Saville JW, Zhu X, Srivastava SS, Berezuk AM, Tuttle KS, et al. SARS-CoV-2 Omicron variant: Antibody evasion and cryo-EM structure of spike protein-ACE2 complex. Science. 2022; 375 (6582):760–4. Epub 2022/01/21. https://doi.org/10.1126/science.abn7760 PMID: 35050643.

51. Schmidt F, Muecksch F, Weisblum Y, Da Silva J, Bednarski E, Cho A, et al. Plasma Neutralization of the SARS-CoV-2 Omicron Variant. New England Journal of Medicine. 2022; 386(6):599–601. Epub 2022/01/15. https://doi.org/10.1056/NEJMc2119641 PMID: 35030645; PubMed Central PMCID: PMC8757565.

52. Juno JA, Tan HX, Lee WS, Reynaldi A, Kelly HG, Wragg K, et al. Humoral and circulating follicular helper T cell responses in recovered patients with COVID-19. Nat Med. 2020; 26(9):1428–34. Epub 2020/07/15. https://doi.org/10.1038/s41591-020-0995-0 PMID: 32661393.

53. Zuo Y, Estes SK, Ali RA, Gandhi AA, Yalavarthi S, Shi H, et al. Prothrombotic autoantibodies in serum from patients hospitalized with COVID-19. Sci Transl Med. 2020; 12(570). Epub 2020/11/04. https://doi.org/10.1126/scitranslmed.abd3876 PMID: 33139519; PubMed Central PMCID: PMC7724273.

54. Bastard P, Rosen LB, Zhang Q, Michailidis E, Hoffmann HH, Zhang Y, et al. Autoantibodies against type I IFNs in patients with life-threatening COVID-19. Science. 2020; 370(6515). Epub 2020/09/26. https://doi.org/10.1126/science.abd4585 PMID: 32972996; PubMed Central PMCID: PMC7857397.

55. Zuniga M, Gomes C, Carsons SE, Bender MT, Cotzia P, Miao QR, et al. Autoimmunity to the Lung Protective Phospholipid-Binding Protein Annexin A2 Predicts Mortality Among Hospitalized COVID-19 Patients. medRxiv. 2021. https://doi.org/10.1101/2020.12.28.20248807

56. Agrawal G, Holt T, Suresh B, Chir W, Van der Veken L. The COVID-19 vaccines are here: What comes next?.

57. Capua I, Giaquinto C. The unsung virtue of thermostability. Lancet. 2021; 397(10282):1346. Epub 2021/03/27. https://doi.org/10.1016/S0140-6736(21)00526-2 PMID: 33770518; PubMed Central PMCID: PMC7987303.

58. Nachega JB, Sam-Agudu NA, Mellors JW, Zumla A, Mofenson LM. Scaling Up Covid-19 Vaccination in Africa—Lessons from the HIV Pandemic. New England Journal of Medicine. 2021. Epub 2021/04/01. https://doi.org/10.1056/NEJMp2103313 PMID: 33789005.

59. Xiong S, Gerloni M, Zanetti M. Engineering vaccines with heterologous B and T cell epitopes using immunoglobulin genes. Nature Biotech. 1997; 15:882–6. https://doi.org/10.1038/nbt0997-882 PMID: 9306404

60. Sollazzo M, Hasemann CA, Meek KD, Glotz D, Capra JD, Zanetti M. Molecular characterization of the VH region of murine autoantibodies from neonatal and adult BALB/c mice. Eur J Immunol. 1989; 19 (3):453–7. https://doi.org/10.1002/eji.1830190307 PMID: 2495969

61. Liu P, Zhu F, Rassokhin DN, Agrafiotis DK. A self-organizing algorithm for modeling protein loops. PLoS Comput Biol. 2009; 5(8):e1000478. Epub 2009/08/22. https://doi.org/10.1371/journal.pcbi.1000478 PMID: 19696883; PubMed Central PMCID: PMC2719875.